Perpendicular magnetic anisotropy induced by antiferromagnetic Mn-Pd alloy films: Dual effects of exchange and spin-orbit coupling

Bo-Yao Wang [1,*] Jie-Ying Lee,[1] Wan-Lin Li,[1] Kai Lin,[1] Ming-Shian Tsai,[1,2]
Tzu-Hung Chuang,[3] and Der-Hsin Wei [3]

[1]*Department of Physics, National Changhua University of Education, Changhua 500, Taiwan*
[2]*Institute of Photonics Technologies, National Tsing Hua University, Hsinchu 300, Taiwan*
[3]*National Synchrotron Radiation Research Center, Hsinchu 300, Taiwan*

Ferromagnetic (FM) films with perpendicular magnetic anisotropy (PMA) are crucial building blocks of state-of-the-art perpendicular magnetic devices. This study investigated the effects of triggering PMA in FM thin films by applying $Mn_{1-x}Pd_x$-based antiferromagnetic (AFM) thin films with strong AFM exchange coupling from Mn and high spin-orbit coupling from Pd atoms. Our results reveal that $Mn_{1-x}Pd_x$ films can trigger PMA in Co/Ni films with weak in-plane magnetic anisotropy at room temperature through either $Mn_{1-x}Pd_x$-facilitated interfacial perpendicular crystalline anisotropy (spin-orbit coupling, $x \geqslant 10\%$) or incorporation of them with antiferromagnet-induced exchange coupling ($x \leqslant 10\%$). In Co/Fe films with strong in-plane magnetic anisotropy, Mn-rich $Mn_{1-x}Pd_x$ films ($x \leqslant 10\%$) can induce stable PMA at low temperatures through concurrently enhanced spin-orbit coupling and antiferromagnet-induced exchange coupling across the AFM–FM interface. Our research clarifies the dual effects of exchange and spin-orbit coupling in $Mn_{1-x}Pd_x$ films, which trigger the PMA of adjacent FM films. This indicates that $Mn_{1-x}Pd_x$ films are promising candidates for achieving controllable PMA.

I. INTRODUCTION

Perpendicular magnetic anisotropy (PMA) is the core of state-of-the-art magnetic devices, such as spin-transfer torque magnetic random memory, and aids in increasing magnetic storage density, reading and writing speeds, and reducing energy consumption [1–6]. PMA can be achieved in a ferromagnetic (FM) layer through the use of crystal-distorted alloy films or multilayers composed of both FM materials and noble metals, such as Pt and Pd [7–11]. Due to the asymmetry of the crystal field in these structures, the valence orbitals of noble metals with higher spin-orbit coupling constants can cause perpendicular crystalline anisotropy of adjacent FM atoms or films through orbital hybridization [12]. Antiferromagnetic (AFM) thin films are emerging materials that can potentially trigger PMA in FM films through AFM–FM exchange coupling [13–20]. Because of this exchange coupling, the PMA induced by an AFM film is sensitive to not only the spin structure at the AFM–FM interface [18,19] but also the thickness and temperature [20–22] of the AFM material, which are determined by its finite-size effect [23]. AFM face-centered-cubic (fcc) $Fe_{0.5}Mn_{0.5}$ with a three-dimensional quadratic-type [24–27] or a vertically expanded face-centered tetragonal (e-fct) Mn film with a two-dimensional layered spin structures [28,29] can trigger PMA in FM Co/Ni(Fe) films through collinearlike or noncollinear-type exchange coupling [17–20]. Because noble metals and AFM films trigger PMA through different mechanisms, a combination of these two

materials can provide an additional degree of freedom in controlling PMA and complement existing mechanisms. To date, however, antiferromagnet-induced PMA has mostly been examined in $3d$-based AFM–FM systems [17–20]. To facilitate the development of potential applications for perpendicular magnetic devices, how AFM–noble-metal alloy films can induce PMA in FM films should be investigated.

AFM Mn–Pd alloy films with sizable AFM moments contributed by Mn atoms and the high valence orbitals of Pd atoms are promising candidates for examining the dual effects of exchange and spin-orbit coupling on PMA induction. Bulk $Mn_{0.5}Pd_{0.5}$ exhibits an $L1_0$-type vertically contracted face-centered-tetragonal (c-fct) structure with the lattice constants $a = b = 4.07$ Å and $c = 3.58$ Å [30], and Mn and Pd atoms occupy alternating atomic sheets perpendicular to the c axis [Fig. 1(a)]. Neutron scattering experiments [31,32] have revealed that c-fct $Mn_{0.5}Pd_{0.5}$ exhibits a fully compensated spin configuration on the surface perpendicular to the c axis; although a sizable magnetic moment of 4.4 μ_b/atom was detected for Mn, a small value was observed for Pd (<0.25 μ_b/atom) [31–33]. When grown on a MgO(001) substrate, $Mn_{0.5}Pd_{0.5}$ films have exhibited either a c-axis-grown [Fig. 1(a)] or e-fct (a-axis-grown) structure [Fig. 1(b)], depending on growth temperature [34–37]. In e-fct $Mn_{0.5}Pd_{0.5}$ films [Fig. 1(b)], Mn and Pd atomic sheets are perpendicular to the substrate surface, forming a c(2×2)-ordered atomic structure in each layer. Therefore, in an e-fct $Mn_{0.5}Pd_{0.5}$/FM bilayer, interfacial Mn and Pd atoms can induce both exchange and spin-orbit coupling in the adjacent FM film. In addition, e-fct $Mn_{0.5}Pd_{0.5}$ exhibits an uncompensated in-plane spin configuration on the surface and at the interface
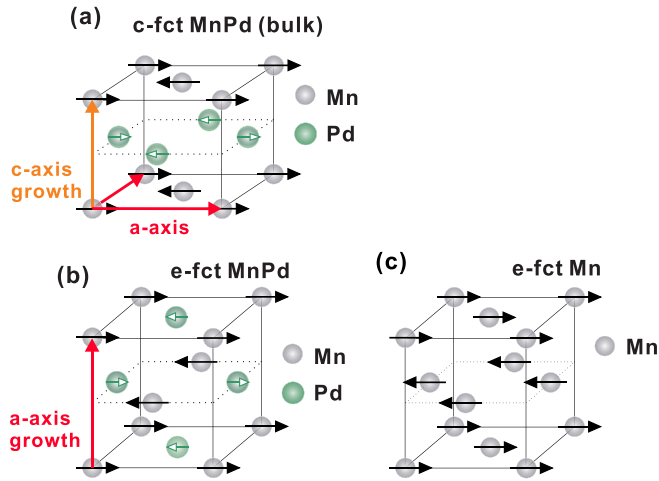
*bywang1735@cc.ncue.edu.tw

FIG. 1. Illustration of the atomic and spin structures of (a) c-axis-grown (or c-fct) $Mn_{0.5}Pd_{0.5}$, (b) a-axis-grown (or e-fct) $Mn_{0.5}Pd_{0.5}$, and (c) e-fct Mn films [28–30,34].

[Fig. 1(b)] [34,37], where the in-plane spin orientation of Mn moments is similar to that of Mn moments in e-fct Mn/Co/Cu(001) [Fig. 1(c)] [28,29]. Therefore, a comparison of a series of $Mn_{1-x}Pd_x$ films grown on structurally coherent Co/Ni(Fe)/Cu(001) with different levels of Pd alloying can reveal the effects of exchange and spin-orbit coupling as well as their interplay on the PMA of adjacent FM films.

In this study, we comprehensively examined the conditions and mechanisms crucial for triggering PMA in a series of $Mn_{1-x}Pd_x$/Co/Ni(Fe)/Cu(001) films with various thicknesses and AFM alloy concentrations at different temperatures. We determined that $Mn_{1-x}Pd_x$ films can trigger PMA in adjacent Co/Ni(Fe)/Cu(001) films with different levels of in-plane magnetic anisotropy [11,20,38–40] through $Mn_{1-x}Pd_x$-facilitated interfacial perpendicular crystalline anisotropy (spin-orbit coupling, $x \geqslant 10\%$) or incorporation of them with antiferromagnet-induced exchange coupling ($x \leqslant 10\%$). Our findings demonstrate the dual effects of the exchange and spin-orbit coupling of $Mn_{1-x}Pd_x$ films in triggering PMA in adjacent FM films, indicating that a combination of a noble metal and 3*d* element can provide an additional degree of freedom for controlling PMA through the use of AFM films.

II. EXPERIMENT

We grew a series of $Mn_{1-x}Pd_x$ films on two-monolayer (ML) Co/14-ML Ni/Cu(001) (Co/Ni/Cu) and 3-ML Co/3-ML Fe/Cu(001) (Co/Fe/Cu) films in a multifunctional ultrahigh-vacuum chamber (base pressure of 2×10^{-10} Torr). All the films were deposited using e-beam evaporators at room temperature. We employed five electron beam evaporators to deposit the various elements. Rod-shaped sources were used for Fe, Co, and Ni, while Mn and Pd were placed in Mo crucibles. Cu(001) substrates with a miscut angle of $<0.1°$ were subjected to cycles of 2-keV Ar$^+$ ion sputtering and 5 min of subsequent annealing at 800 K to ensure a well-ordered crystalline structure and smooth surface. The $Mn_{1-x}Pd_x$ films were prepared through the codeposition of Mn and Pd with

respective evaporators, and the alloy compositions were controlled through adjustment of the deposition rates on the basis of the oscillation of their medium-energy electron diffraction (MEED) curves [41]. As depicted in Fig. S1 of the Supplemental Material [41] the MEED curves of the $Mn_{1-x}Pd_x$ films grown on Co/Ni/Cu or Co/Fe/Cu exhibited regular oscillation, indicating successful layer-by-layer growth. The average in-plane and vertical interlayer distances of the films were determined *in situ* through low-energy electron diffraction (LEED) with kinematics approximation (LEED I/V) at room temperature. Figure S2 of the Supplemental Material [41] shows that the LEED p(1×1) spots of 1,2 ML $Mn_{1-x}Pd_x$/Co/Ni/Cu (x = 0.1–0.5%) are located at the same positions as the Co/Ni/Cu and the Cu(001) substrate, indicating the epitaxial growth of these thin $Mn_{1-x}Pd_x$ films on Co/Ni/Cu. In addition, the $Mn_{1-x}Pd_x$ films exhibited an e-fct structure (c/a ≈ 1.04) on the Co/Ni(Fe)/Cu when Pd concentration was $\leqslant 10\%$ and the $Mn_{1-x}Pd_x$ thickness (t_{MnPd}) was $\geqslant 6(5)$ ML [Figs. S3 and S4 of Supplemental Material [41]]; this e-fct structure remained consistent for t_{MnPd} within the range of 5–10 ML, indicating that it is one of the stable structures for Mn-rich $Mn_{1-x}Pd_x$ films. When the Pd concentration in the $Mn_{1-x}Pd_x$/Co/Ni(Fe)/Cu was $>$ 10%, constructive interference peaks in the LEED IV curves were observed when t_{MnPd} was $<$ 4 ML [41]. This finding indicates that the $Mn_{1-x}Pd_x$ films with Pd concentration $>$ 10% and $t_{MnPd} \geqslant 4$ ML can be structurally disordered, possibly due to the large lattice mismatch between these $Mn_{1-x}Pd_x$ and Cu(001) [30,42–44].

The in-plane and out-of-plane magnetic hysteresis loops of the films were determined using longitudinal and polar magneto-optical Kerr effect (MOKE) measurements, respectively, performed *in situ* at either 300 or 155 K, or systematically varied from 155 to 300 K. In the longitudinal mode, the magnetic field direction is parallel to the film surface, while in the polar mode it is perpendicular. The laser beam angle relative to the sample was kept at 45° in both modes, and the signals were measured using a photomodulator and lock-in technique. In addition, we performed x-ray magnetic circular dichroism (XMCD) analysis [45] at Co and Mn $L_{3,2}$ absorption edges to investigate the magnetic properties of the interfacial Co and Mn layers in $Mn_{1-x}Pd_x$/Co/Ni/Cu; these x-ray measurements were performed *in situ* in the end station of an x-ray photoemission electron microscope (PEEM) [46–48] in beamline BL05B2 of the Taiwan Light Source at the National Synchrotron Radiation Research Center. The x-ray absorption spectrum (XAS) and XMCD curves were measured in the total electron yield mode and normalized relative to the incident beam intensity and the $L_{3,2}$ edge jump. The XAS and XMCD curves were measured under remanent conditions. Two remanent states were generated by applying positive or negative magnetic fields along the in-plane (± 200 Oe) or out-of-plane (± 1000 Oe) directions to the magnetic samples.

III. RESULTS

A. PMA in $Mn_{1-x}Pd_x$/Co/Ni/Cu(001)

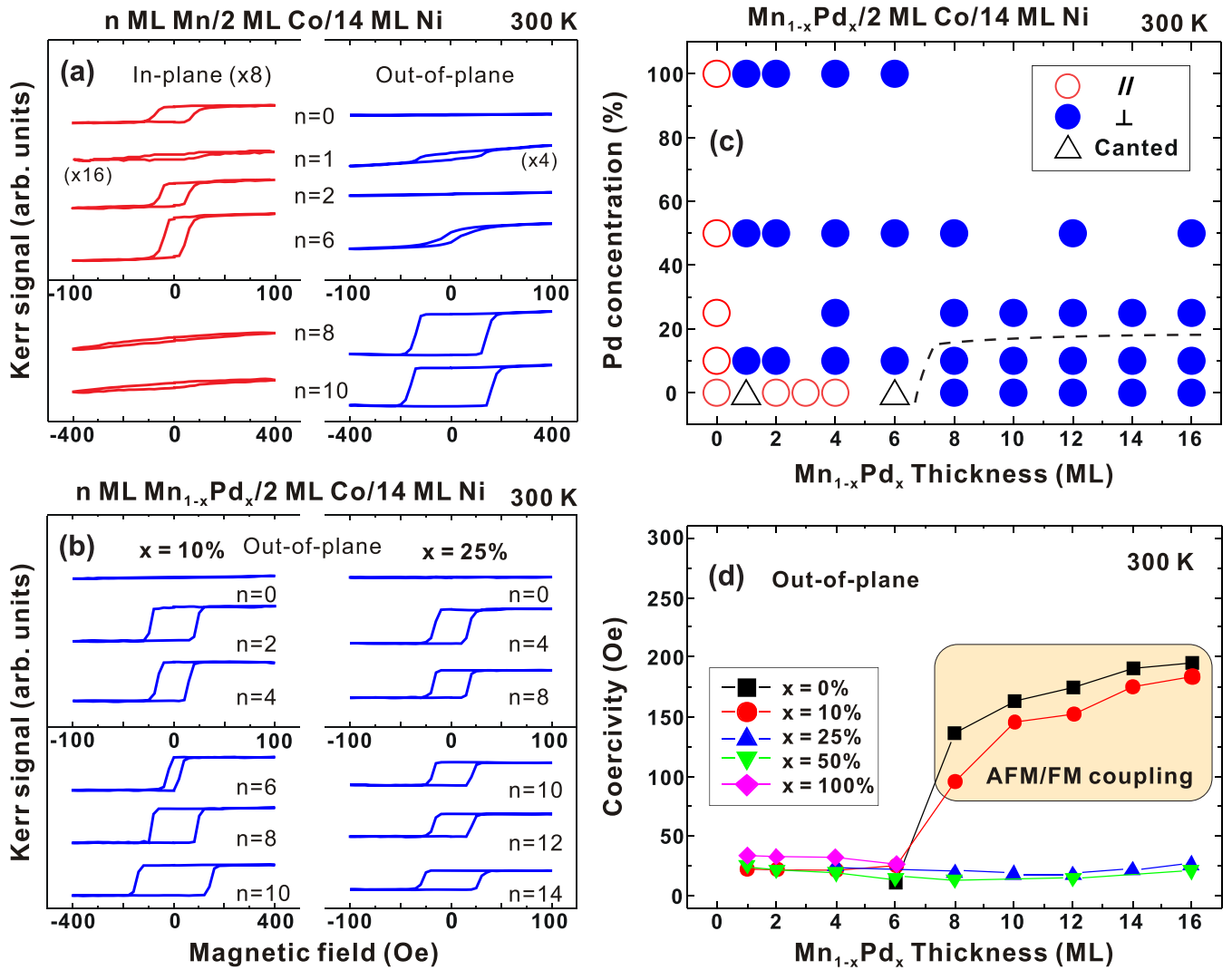We investigated the effects of $Mn_{1-x}Pd_x$ films on PMA induction in the adjacent Co/Ni/Cu with a lower total

FIG. 2. Magnetic hysteresis loops of (a) Mn/Co/Ni/Cu and (b) $Mn_{1-x}Pd_x$/Co/Ni/Cu (Pd concentration (x) = 10% and 25%) with various t_{Mn} and t_{MnPd}, respectively, determined from the longitudinal and polar MOKE at 300 K. (c), (d) Summarized magnetic easy-axis phase diagram and perpendicular H_c of $Mn_{1-x}Pd_x$/Co/Ni/Cu measured at 300 K. In (c), the symbols ∥ and ⊥, respectively, denote the in-plane and perpendicular magnetic easy directions of $Mn_{1-x}Pd_x$/Co/Ni/Cu. The yellow shadow in (d) (dashed-line region of (c); $t_{Mn}(t_{MnPd}) > 6$ ML, $x \leqslant 10\%$) shows perpendicularly magnetic $Mn_{1-x}Pd_x$/Co/Ni/Cu exhibiting a higher H_c value, for which the long-range AFM ordering of $Mn_{1-x}Pd_x$ was established. In contrast, $Mn_{1-x}Pd_x$ films with other t_{MnPd} or alloy compositions remained in a paramagnetic state.

in-plane magnetic anisotropy energy density (-0.64 mJ/m^2) [11,38,39,41] by examining the MOKE at 300 K. Figure 2(a) presents the magnetic hysteresis loops of the Mn/Co/Ni/Cu films with various Mn thicknesses (t_{Mn}). The Co/Ni/Cu exhibited in-plane magnetic anisotropy. Moreover, tilted magnetization with coexisted in-plane and out-of-plane magnetic hysteresis loops was observed in 1-ML Mn/Co/Ni/Cu. As no additional structures were observed in 1-ML Mn/Co/Ni/Cu when compared to Co/Ni layer [17], we can conclude that the tilted magnetization induced in 1-ML Mn/Co/Ni/Cu may be caused by the interface effect of the Mn film. In addition, robust PMA with a sizable H_c was observed in the Mn/Co/Ni/Cu films with $t_{Mn} > 6$ ML. When the Pd concentration in $Mn_{1-x}Pd_x$ was increased to 10% and 25% [Fig. 2(b)], perpendicular magnetization was observed in both thin $Mn_{1-x}Pd_x$ films ($t_{MnPd} < 6$ ML) and the thicker $Mn_{1-x}Pd_x$ films. Additionally, in $Mn_{0.9}Pd_{0.1}$/Co/Ni/Cu,

PMA with significantly increased coercivity H_c was observed when $t_{MnPd} > 6$ ML.

Figure 2(c) illustrates the complete magnetic easy-axis phase diagram for the $Mn_{1-x}Pd_x$/Co/Ni/Cu films, including the Pd concentration and t_{MnPd} dependence. PMA was triggered in all films (Pd concentrations of 0%–100%) except for thin Mn/Co/Ni/Cu films ($t_{Mn} < 6$ ML). According to the literature [38,39,41], increasing the tensile strain of the fcc-like Co layer can strengthen the in-plane anisotropy due to the negative magneto-elastic anisotropy constant (K_{me}) (as seen in Co/Cu(001) with a strain of 2% and K_{me} of -73.8 μeV/atom). Conversely, increasing the tensile strain of the fcc-like Ni layer has inverse effects due to a positive K_{me} of 29 μeV/atom (as observed in Ni/Cu(001) with a strain of 2.6%). Therefore, in an epitaxially grown Co/Ni/Cu film, the magnetoelastic anisotropy effects on Co and Ni can offset each other based on their relative thicknesses. In this study, Mn-rich $Mn_{1-x}Pd_x$

or thin Pd-rich $Mn_{1-x}Pd_x$ ($t_{MnPd} < 4$ ML) films were epitaxially grown on Co/Ni/Cu [Figs. S3 and S4 of Supplemental Material [41]]. The lattice constant of these Co/Ni films is identical to that of Cu(001), resulting in similar strain levels for Co and Ni in the $Mn_{1-x}Pd_x$/Co/Ni/Cu films as in Co/Ni/Cu alone (2% for Co and 2.6% for Ni). Therefore, any PMA induced in either Mn-rich $Mn_{1-x}Pd_x$/Co/Ni/Cu or thin Pd-rich $Mn_{1-x}Pd_x$/Co/Ni/Cu ($t_{MnPd} < 4$ ML) films should not be attributed to additional strain effects on the Co/Ni/Cu films.

To understand the origin of the PMA in the $Mn_{1-x}Pd_x$/Co/Ni/Cu films, it was crucial to determine the onset of long-range AFM ordering in the $Mn_{1-x}Pd_x$ films. Previous studies [49–53] utilized x-ray magnetic linear dichroism (XMLD) as a direct method for examining the long-range AFM order in AFM films. However, obtaining distinguishable XMLD spectra for the current AFM films was challenging due to the fixed orientation between the x-ray and sample holder and the full magnetic shielding in the sample holder of the PEEM [48]. Therefore, in this work, we characterized the onset of long-range AFM ordering in the $Mn_{1-x}Pd_x$ films by observing the fingerprintlike phenomenon of increased H_c in the coupled AFM/FM systems. This approach has been justified in numerous previous studies [54–57]. We observed that in the Mn/Co/Ni/Cu or $Mn_{0.9}Pd_{0.1}$/Co/Ni/Cu films, the perpendicular magnetization was accompanied by strong H_c enhancement when t_{Mn} or t_{MnPd} was > 6 ML [Fig. 2(d)]. This behavior suggests that long-range AFM ordering of Mn or $Mn_{0.9}Pd_{0.1}$ films is established when t_{Mn} or t_{MnPd} is > 6 ML. However, unlike the Mn/Co/Ni/Cu films [Fig. 2(a)], even very thin $Mn_{0.9}Pd_{0.1}$ films ($t_{MnPd} = 1$ ML) [Fig. 2(c)] can trigger PMA on adjacent Co/Ni/Cu. Since the induced PMA in thin $Mn_{0.9}Pd_{0.1}$/Co/Ni/Cu films ($t_{MnPd} < 6$ ML; $H_c < 40$ Oe) exhibits a significantly lower H_c value than thick $Mn_{0.9}Pd_{0.1}$/Co/Ni/Cu films ($t_{MnPd} > 6$ ML; $H_c > 100$ Oe), it can be inferred that the thin $Mn_{0.9}Pd_{0.1}$ films remained in a paramagnetic state. Similarly, PMA and a low perpendicular H_c value ($H_c < 40$ Oe) were observed in the $Mn_{1-x}Pd_x$/Co/Ni/Cu films when Pd concentration was $> 10\%$ [Fig. 2(d)]. Since no H_c enhancement behavior was observed in $Mn_{1-x}Pd_x$/Co/Ni/Cu with x $> 10\%$ in the entire thickness region of t_{MnPd} measured in this work, we can also infer that these $Mn_{1-x}Pd_x$ films with $x > 10\%$ remained in a paramagnetic state. Therefore, the PMA induced in $Mn_{1-x}Pd_x$ films with $x > 10\%$ was likely attributable not to antiferromagnet-induced exchange coupling but to $Mn_{1-x}Pd_x$-facilitated interface effects.

B. $Mn_{1-x}Pd_x$-facilitated interfacial perpendicular crystalline anisotropy and exchange coupling

To investigate the impact of $Mn_{1-x}Pd_x$ on the PMA of $Mn_{1-x}Pd_x$/Co/Ni/Cu films, we performed Co, Mn $L_{3,2}$ edges XAS, and XMCD measurements. Previous study by Bruno [58] have shown that the magnetic anisotropy due to spin-orbit coupling, i.e., magnetocrystalline anisotropy, is proportional to the anisotropy of the orbital moment ($m_{orbital}$). However, the error in the orbital sum rule calculation is twice the $m_{orbital}/m_{spin}$ ratio due to the requirement for accurate

values of the circular polarization level of light, the angle between light and magnetic moment, and the exact $3d$ unoccupied state value [45]. On the other hand, Stöhr and König have demonstrated that in the presence of spin-orbit coupling, the spin moment (m_{spin}) for $3d$ transition metals remains isotropic to a significant extent. This finding is supported by XMCD experiments and DFT calculations on Co/Pd multilayers [33,59]. Therefore, the angular-dependent ratio of $m_{orbital}/m_{spin}$ can serve as useful information for probing the magnetocrystalline anisotropy of $3d$ magnetic films. In this study, due to the restricted orientation between the x-ray and sample holder and full magnetic shielding in the sample holder of the PEEM [48], we indirectly estimated the anisotropy of $m_{orbital}/m_{spin}$ ratios from the values of in-plane magnetic Co/Ni/Cu film ($m_{orbital}^{\parallel}/m_{spin}$) [Fig. 3(a)] and perpendicularly magnetic $Mn_{1-x}Pd_x$/Co/Ni/Cu samples ($m_{orbital}^{\perp}/m_{spin}$) [Figs. 3(b), 3(c), 3(e), and 3(f)]. The ratio of the orbital-to-spin moments can be obtained as $m_{orbital}/m_{spin} = 2q/(9p-6q)$ according to the XMCD sum rules [45] and the assumption of a negligible magnetic dipole operator for the spin sum rule (a reasonable assumption for $3d$ metals) [60–62]. The p and q values were determined through the integration of the L_3 and $L_3 + L_2$ regions.

Compared with the $m_{orbital}^{\parallel}/m_{spin}$ value of in-plane magnetic Co/Ni/Cu (approximately 0.11), the $m_{orbital}^{\perp}/m_{spin}$ ratio of the various perpendicularly magnetic $Mn_{1-x}Pd_x$/Co/Ni/Cu films was higher, at 0.17–0.13 [Fig. 3]. This finding indicates an increase in the perpendicular crystalline anisotropy of the Co layer in these perpendicularly magnetic systems [58] resulting from orbital hybridization and spin-orbit coupling at the $Mn_{1-x}Pd_x$–Co interface. In addition, compared with the Mn-rich $Mn_{1-x}Pd_x$/Co/Ni/Cu films [Figs. 3(e), 3(f)], the Pd-rich $Mn_{1-x}Pd_x$/Co/Ni/Cu films exhibited greater $m_{orbital}^{\perp}/m_{spin}$ ratios of Co moments [Fig. 3(b)]. The Stoner-Wohlfarth model [63] states that a magnetic system with giant uniaxial magnetocrystalline anisotropy can result in an enhanced H_c along the magnetic easy direction, given by the equation $H_c = 2K_{cry}/\mu_0 M_s$, where K_{cry} is the uniaxial magnetocrystalline anisotropy, μ_0 is the vacuum permeability, and M_s is the saturation magnetization dominated by m_{spin}. For a magnetic system with giant uniaxial crystalline anisotropy (such as PMA), there exists a roughly proportional relationship $H_c \propto m_{orbital}/m_{spin}$ at the magnetic easy direction. In this study, both Pd and $Mn_{0.5}Pd_{0.5}$ films are in a paramagnetic state as shown in Fig. 2(d). However, compared to $Mn_{0.5}Pd_{0.5}$/Co/Ni/Cu, the Pd/Co/Ni/Cu films exhibit concurrently enhanced $m_{orbital}^{\perp}/m_{spin}$ ratios of Co moments and perpendicular H_c [Figs. 3(b)–3(d)]. This suggests that $Mn_{1-x}Pd_x$ films with higher Pd concentrations can generate stronger interfacial perpendicular crystalline anisotropy on the adjacent Co layer. According to the literature [12,64], the crystalline anisotropy induced by spin-orbit coupling is proportional to the square of the spin-orbit coupling constant, which is larger for elements with higher atomic numbers. Thus, in the present case, the $4d$ Pd atoms at the interface could engender stronger perpendicular crystalline anisotropy than did the $3d$ Mn atoms. This result is supported by a finding of a lack of PMA in a similar $Ni_{0.5}Mn_{0.5}$/Co/Ni/Cu film [19], where the spin-orbit coupling constant of $3d$ Ni was also smaller
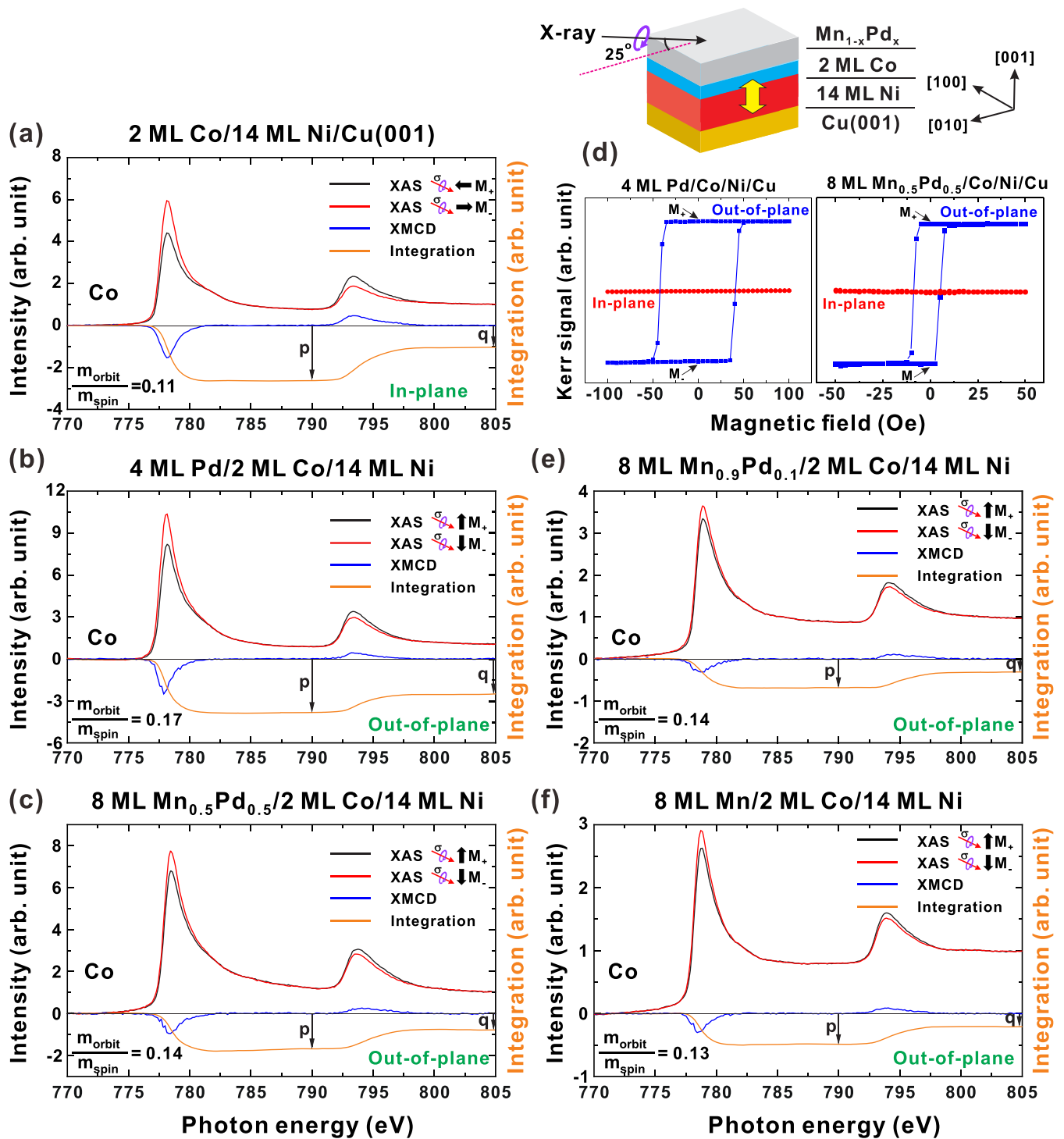
FIG. 3. XAS and XMCD curves of (a) Co/Ni/Cu, (b) 4-ML Pd/Co/Ni/Cu, and (c) 8-ML $Mn_{0.5}Pd_{0.5}$/Co/Ni/Cu measured at Co $L_{3,2}$ edges and 300 K in remanent states. (d) In-plane and out-of-plane magnetic hysteresis loops of 4-ML Pd/Co/Ni/Cu and 8-ML $Mn_{0.5}Pd_{0.5}$/Co/Ni/Cu measured at 300 K. (e), (f) XAS and XMCD curves of 8-ML $Mn_{0.9}Pd_{0.1}$/Co/Ni/Cu and 8-ML Mn/Co/Ni/Cu measured at Co $L_{3,2}$ edges and 300 K in remanent states. The illustrations in the top right of the figures indicate the geometry of the XMCD measurements in the PEEM end station [48]. σ denotes the photo helicity of incident X-ray. The bold black arrows indicate the remanent states of the films (M_+ or M_-) under positive or negative magnetic fields. The orbital-to-spin ratios ($m_{orbital}/m_{spin}$) of Co moments were determined from XMCD curves in accordance with XMCD sum rules [45].

than that of $4d$ Pd atoms [12]. It is noteworthy that the Mn/Co/Ni/Co/Cu film exhibits a higher $m_{orbital}^{\perp}/m_{spin}$ ratio of Co moments (0.13) compared to the in-plane magnetic Co/Ni/Cu film ($m_{orbital}^{\parallel}/m_{spin} = 0.11$). This observation

suggests that the Mn-Co interface in Mn/Co/Ni/Cu can also induce perpendicular crystalline anisotropy in the Co layer, as reported in the literature [65]. However, because the interfacial perpendicular crystalline anisotropy induced by

Mn was weaker than that induced by Pd, the effect could only slightly tilt the magnetization of the 1-ML Mn/Co/Ni/Cu [Fig. 2(a)]. Stable PMA with a large H_c value can be triggered by an AFM Mn film through antiferromagnet-induced exchange coupling only when $t_{Mn} > 6$ ML.

To investigate the interface coupling in $Mn_{1-x}Pd_x$/Co/Ni/Cu films with induced PMA, Mn $L_{3,2}$ XAS and XMCD curves were measured. In the perpendicularly magnetic 8-ML $Mn_{0.5}Pd_{0.5}$/Co/Ni/Cu with the $Mn_{0.5}Pd_{0.5}$ film in a paramagnetic state, a slight XMCD signal was detected for the Mn element [Fig. 4(a)]. This small Mn XMCD signal is likely due to an interface-polarized effect of the Co on the paramagnetic Mn moments, as has been observed in paramagnetic Mn-based alloy/Co films [66]. By contrast, in 8-ML $Mn_{0.9}Pd_{0.1}$/Co/Ni/Cu [Fig. 4(b)] and 8-ML Mn/Co/Ni/Cu films [Fig. 4(c)], for which long-range AFM ordering was established, significantly reduced XMCD signal was detected for the Mn element, despite distinct perpendicular magnetization observed by MOKE [Fig. 4(d)] and Co XMCD [Figs. 3(e) and 3(f)]. These results suggest that in the perpendicularly magnetic 8-ML $Mn_{0.9}Pd_{0.1}$/Co/Ni/Cu and 8-ML Mn/Co/Ni/Cu films, the out-of-plane component of the uncompensated Mn moments flips very little under the flipping of the perpendicular magnetization of Co/Ni/Cu and the out-of-plane magnetic field. This behavior is in contrast to the sizable uncompensated Mn moments observed in perpendicularly magnetic $Fe_{0.5}Mn_{0.5}$/Co/Ni/Cu films with collinearlike coupling at the interface [18]. Spin-polarized scanning tunneling microscopy measurements have verified an in-plane layered-AFM spin structure for the top layer of Mn/Co/Cu(001) [Fig. 1(c)] [28,29], and the in-plane oriented spin structure of $Mn_{0.5}Pd_{0.5}$ has been detected by neutron scattering experiments [Fig. 1(a)] [31,32]. Given the similar lattice structure and magnetic behavior observed between $Mn_{0.9}Pd_{0.1}$/Co/Ni/Cu and Mn/Co/Ni/Cu [41], we speculate that these 10% Pd atoms may only substitute the Mn atoms without significantly changing the in-plane orientation of Mn moments. Therefore, combining the previous results and the current study, we suggest that $Mn_{0.9}Pd_{0.1}$(Mn) at the interface of $Mn_{0.9}Pd_{0.1}$(Mn)/Co/Ni/Cu not only enhances the perpendicular crystalline anisotropy of the adjacent Co film [Figs. 3(e) and 3(f)] but also couples noncollinearly with the adjacent Co/Ni layers [Fig. 4(e)], triggering the establishment of PMA. To summarize the results so far, our results indicate that $Mn_{1-x}Pd_x$ films can trigger PMA in adjacent Co/Ni/Cu at room temperature through $Mn_{1-x}Pd_x$-facilitated perpendicular crystalline anisotropy (spin-orbit coupling; $x \geqslant 10\%$). Moreover, thicker Mn-rich ($x \leqslant 10\%$) $Mn_{1-x}Pd_x$ films with long-range AFM ordering result in stronger PMA due to antiferromagnet-induced noncollinear exchange coupling.

C. PMA in $Mn_{1-x}Pd_x$/Co/Fe/Cu(001)

To explore the impact of $Mn_{1-x}Pd_x$ films on inducing PMA in FM films with higher in-plane magnetic anisotropy, we investigated $Mn_{1-x}Pd_x$/Co/Fe/Cu films. The total in-plane magnetic anisotropy energy density of the Co/Fe/Cu alone was approximately -1.4 mJ/m^2 [20,40,41]. Figure 5(a) depicts the magnetic hysteresis loops of 0–8-ML

Mn/Co/Fe/Cu films measured at 155 K (PMA was not observed at room temperature). The Co/Fe/Cu exhibited stable in-plane magnetic anisotropy, and PMA was observed for $t_{Mn} > 4$ ML. Because the perpendicular magnetization was accompanied by strong H_c enhancement, the established long-range AFM ordering and antiferromagnet-induced exchange coupling were inferred to contribute to the PMA. For the $Mn_{0.9}Pd_{0.1}$/Co/Fe/Cu films, similar behaviors of PMA induction and H_c enhancement were observed when t_{MnPd} was > 4 ML [Fig. 5(b)]. This finding indicates that antiferromagnet-induced exchange coupling from the AFM $Mn_{0.9}Pd_{0.1}$ film contributes to PMA induction in $Mn_{0.9}Pd_{0.1}$/Co/Fe/Cu films. However, as displayed in the magnetic easy-axis phase diagram [Fig. 5(c)], PMA was not detected in the $Mn_{0.9}Pd_{0.1}$/Co/Fe/Cu films with $t_{MnPd} = 0$–4 ML or $Mn_{1-x}Pd_x$/Co/Fe/Cu films with Pd concentration $> 10\%$. This result indicates that although $Mn_{1-x}Pd_x$-facilitated interfacial perpendicular crystalline anisotropy alone can successfully stabilize the PMA in the $Mn_{1-x}Pd_x$/Co/Ni/Cu [Fig. 2(c)], it is not sufficient to trigger the perpendicular magnetism in Co/Fe/Cu with strong in-plane magnetic anisotropy. Therefore, in $Mn_{1-x}Pd_x$/Co/Fe/Cu films, PMA must be supported by the antiferromagnet-induced exchange coupling.

D. Competing mechanisms in $Mn_{1-x}Pd_x$-facilitated noncollinear exchange coupling

To further clarify the effects of the antiferromagnet-induced exchange coupling in Mn-rich $Mn_{1-x}Pd_x$/Co/Fe/Cu films that triggers PMA occurs at low temperatures (Fig. 5), we performed temperature-dependent measurements of magnetic hysteresis loops. Figure 6(a) presents the perpendicular magnetic hysteresis loops of the 6-ML and 8-ML Mn/Co/Fe/Cu at different temperatures. The H_c strength increased strongly as temperature decreased. Therefore, the perpendicular magnetization becomes stable at low temperatures. Similar results were observed for the 6-ML and 8-ML $Mn_{0.9}Pd_{0.1}$/Co/Fe/Cu films [Fig. 6(b)].

As mentioned earlier, 6- and 8-ML Mn($Mn_{0.9}Pd_{0.1}$) can induce PMA in Co/Ni/Cu at room temperature [Fig. 2], but only at low temperatures in Co/Fe/Cu [Fig. 6]. Since Mn($Mn_{0.9}Pd_{0.1}$)/Co/Fe/Cu and Mn($Mn_{0.9}Pd_{0.1}$)/Co/Ni/Cu have similar crystal structures, the main difference between these two systems could be the higher in-plane magnetic anisotropy density in Co/Fe/Cu (-1.4 mJ/m^2) [20,40,41] compared to Co/Ni/Cu (-0.64 mJ/m^2) [11,38,39,41]. According to a previous study [20], lowering the sample temperature could enhance the perpendicular crystalline anisotropy at the AFM-Co interface, due to improved crystalline ordering and band narrowing [14,67–69]. Therefore, the establishment of PMA in Mn($Mn_{0.9}Pd_{0.1}$)/Co/Fe/Cu at low temperatures could be due to the concurrent enhancement of perpendicular crystalline anisotropy at the AFM-Co interface and strengthening of the exchange coupling of the AFM Mn($Mn_{0.9}Pd_{0.1}$) moments. However, as shown in Figs. 6(c) and 6(d), the perpendicular H_c value increased with t_{Mn} (or t_{MnPd} in $Mn_{0.9}Pd_{0.1}$/Co/Fe/Cu) in the Mn/Co/Fe/Cu films at a low temperature of T < 185 K (or T < 175 K). By contrast, at a high temperature of T > 185 K (or T > 175 K),
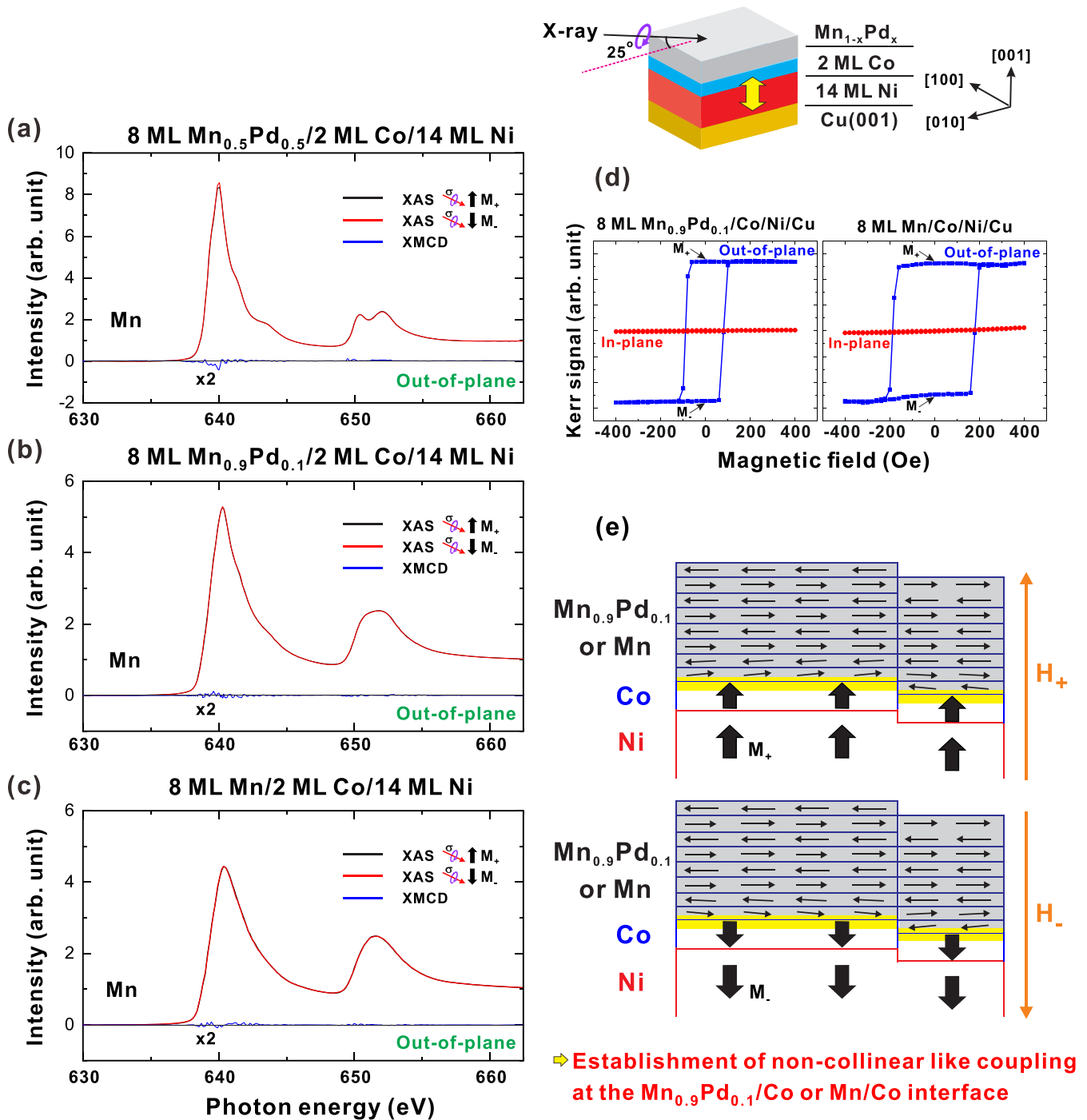
FIG. 4. XAS and XMCD curves of (a) 8-ML $Mn_{0.5}Pd_{0.5}$/Co/Ni/Cu, (b) 8-ML $Mn_{0.9}Pd_{0.1}$/Co/Ni/Cu, and (c) 8-ML Mn/Co/Ni/Cu measured at Mn $L_{3,2}$ edges and 300 K in remanent states. (d) In-plane and out-of-plane magnetic hysteresis loops of 8-ML $Mn_{0.9}Pd_{0.1}$/Co/Ni/Cu and 8-ML Mn/Co/Ni/Cu measured at 300 K. (e) Schematic illustrations of the possible magnetic configurations in 8-ML $Mn_{0.9}Pd_{0.1}$/Co/Ni/Cu and 8-ML Mn/Co/Ni/Cu under positive and negative magnetic fields (H_+ and H_-). In (a)–(c), σ denotes the photo helicity of the incident x-ray, while the bold black arrows (M_+ or M_-) indicate the remanent states of the films under H_+ or H_-. Noted that the yellow color in (e) marks an enhanced perpendicular crystalline anisotropy of the Co layer due to the adjacent $Mn_{0.9}Pd_{0.1}$(Mn) films, as revealed in the results of Fig. 3.

the perpendicular H_c decreased as t_{Mn} (or t_{MnPd}) increased [70]. Since noncollinear exchange coupling between Mn and Co moments has been detected at the interface of Mn($Mn_{0.9}Pd_{0.1}$)/Co/Ni/Cu [Figs. 3 and 4], we speculate that the nontrivial thickness-dependent H_c trends at differ-ent temperatures in Mn($Mn_{0.9}Pd_{0.1}$)/Co/Fe/Cu [Figs. 6(c) and 6(d)] could result from competition between the per-pendicular crystalline anisotropy at the Mn($Mn_{0.9}Pd_{0.1}$)–Co interface and in-plane-oriented AFM coupling from the Mn($Mn_{0.9}Pd_{0.1}$) film with the establishment of noncollinear
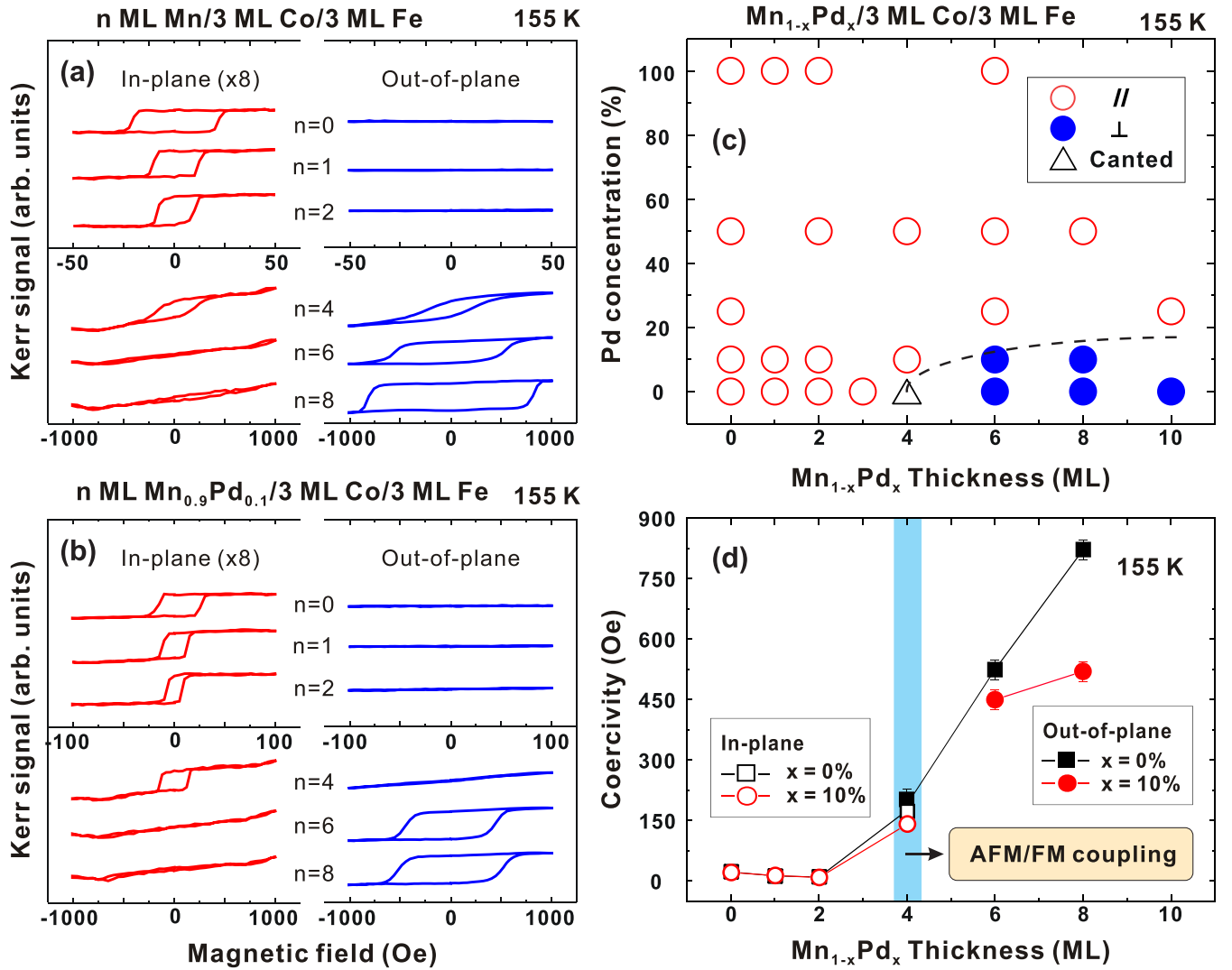
FIG. 5. Magnetic hysteresis loops of (a) 0–8-ML Mn/Co/Fe/Cu and (b) 0–8-ML $Mn_{0.9}Pd_{0.1}$/Co/Fe/Cu determined from the longitudinal and polar MOKE at 155 K. (c) Summarized magnetic easy-axis phase diagram of $Mn_{1-x}Pd_x$/Co/Fe/Cu at 155 K. (d) H_c value of $Mn_{1-x}Pd_x$/Co/Fe/Cu measured at 155 K. In (c), the symbols $\parallel$ and $\perp$, respectively, denote the in-plane and perpendicular magnetic easy directions of the films. The blue shadow in (d) indicates the threshold thickness of Mn-rich $Mn_{1-x}Pd_x$/Co/Ni/Cu exhibiting a high H_c value, with established long-range AFM ordering of $Mn_{1-x}Pd_x$.

exchange coupling. Specifically, at low temperatures, at which the perpendicular crystalline anisotropy of the interfacial moments is robust, the in-plane-oriented AFM moments in the volume of thicker Mn-rich $Mn_{1-x}Pd_x$/Co/Fe/Cu yielded enhanced PMA through noncollinear exchange coupling. In contrast, at higher temperatures, at which the perpendicular crystalline anisotropy of the interfacial moments is weak, noncollinear exchange coupling could be suppressed by the dominant effects of the in-plane lateral exchange coupling of Mn-rich $Mn_{1-x}Pd_x$ moments. Thus, the perpendicular H_c was lower for thicker $Mn_{1-x}Pd_x$. Compared with that of Mn/Co/Fe/Cu [Fig. 6(c)], the perpendicular H_c value of $Mn_{0.9}Pd_{0.1}$/Co/Fe/Cu [Fig. 6(d)] was less sensitive to thickness at both high and low temperatures. This finding suggests that in $Mn_{0.9}Pd_{0.1}$/Co/Fe/Cu, the perturbation of in-plane exchange coupling due to the addition of volume in-plane oriented AFM moments on antiferromagnet-induced noncollinear exchange coupling and PMA are weaker than

those in Mn/Co/Fe/Cu. In the present study, the non-trivial thickness dependence of the perpendicular H_c was observed in Mn-rich $Mn_{1-x}Pd_x$/Co/Fe/Cu but not in Mn-rich $Mn_{1-x}Pd_x$/Co/Ni/Cu, probably because of the highly competitive relationship between the PMA induced by Mn-rich $Mn_{1-x}Pd_x$ and the in-plane magnetic anisotropy of Co/Fe/Cu. However, the same antiferromagnet-induced non-collinear exchange coupling should also be responsible for PMA induction in Mn-rich $Mn_{1-x}Pd_x$/Co/Ni/Cu with weak in-plane anisotropy in the FM film.

IV. DISCUSSION

A. PMA induced in $Mn_{1-x}Pd_x$/Co/Ni(Fe)/Cu(001): Dependence on alloy concentrations

According to the literature, Mn atoms typically exhibit large AFM moments in AFM films, ranging from (4.0–4.4 μ_b/atom), as reported in Refs. [31,32,71,72]. In contrast, Pd
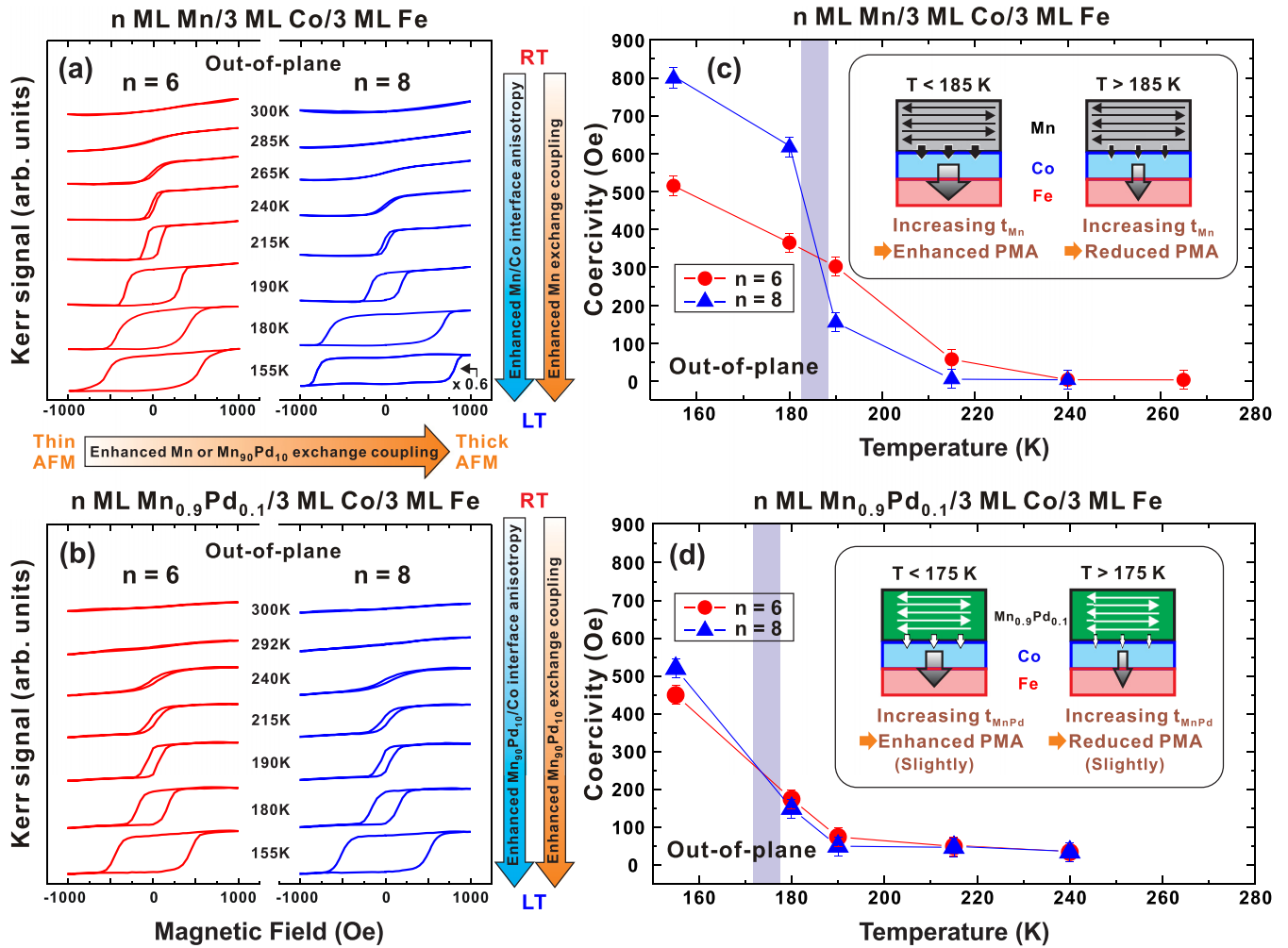
FIG. 6. Perpendicular magnetic hysteresis loops of (a) 6-ML and 8-ML Mn/Co/Fe/Cu and (b) 6-ML and 8-ML $Mn_{0.9}Pd_{0.1}$/Co/Fe/Cu determined from polar MOKE at various temperatures. (c), (d) H_c values based on (a) and (b). Insets illustrate the characteristic noncollinear exchange coupling of these systems with competing mechanisms; perpendicular H_c value increased with t_{Mn} in Mn/Co/Fe/Cu (or t_{MnPd} in $Mn_{0.9}Pd_{0.1}$/Co/Fe/Cu) when T was < 185 K (or< 175 K) but decreased when T was >185 K (or >175 K).

atoms have higher valence orbitals and spin-orbit coupling constants (approximately three times higher than those of Mn atoms) [12], but considerably low spin moments (less than 0.25 μ_b/atom) in Mn-Pd alloys [31–33]. Therefore, in an $Mn_{1-x}Pd_x$/FM bilayer, interfacial Mn and Pd atoms could induce both exchange and spin-orbit coupling in the adjacent FM film.

In the present work, PMA in Co/Ni/Cu could be triggered by $Mn_{1-x}Pd_x$ with a wide range of alloy concentrations. In Pd-rich $Mn_{1-x}Pd_x$ films, in which long-range AFM ordering is not established [73,74], $Mn_{1-x}Pd_x$-facilitated interface crystalline anisotropy contributes to PMA mainly through orbital hybridization and spin-orbit coupling (Figs. 2 and 3). In this study, the strength of $Mn_{1-x}Pd_x$-facilitated perpendicular crystalline anisotropy increased with the Pd concentration because of greater orbital hybridization and spin-orbit coupling [Fig. 3]. However, because of the limited energy of spin-orbit coupling [12], the H_c values of the induced perpendicular magnetization were typically limited to tens of oersteds. In addition, $Mn_{1-x}Pd_x$-facilitated interfacial perpendicular crystalline anisotropy only induced PMA in Co/Ni/Cu, with

its lower total in-plane magnetic anisotropy energy density (-0.64 mJ/m^2) [11,38,39], and was insufficient to trigger PMA in Co/Fe/Cu, with its higher total in-plane anisotropy energy density (-1.4 mJ/m^2) [20,40].

By contrast, the H_c values of perpendicular magnetization induced in Mn-rich $Mn_{1-x}Pd_x$/Co/Ni(Fe)/Cu were typically in the hundreds of oersteds and were dependent on the strength and orientation of the noncollinear exchange coupling established between the interfacial out-of-plane moments [supported by perpendicular crystalline anisotropy and spin-orbit coupling (Fig. 3)] and the volume in-plane moments determined by the AFM structure [Figs. 1(b) and 1(c)] across the AFM–FM interface. In the Mn-rich $Mn_{1-x}Pd_x$/Co/Ni/Cu, with its weak in-plane magnetic anisotropy in the FM film, the H_c of PMA increased with thickness in accordance with the conventional finite-size effects of the AFM film [Fig. 2(d)] [23]. By contrast, with strong in-plane anisotropy in the FM film, the highly competitive nature of the interfacial out-of-plane moments and volume in-plane moments in noncollinear exchange coupling led to the characteristic nontrivial thickness-dependent

H_c [Figs. 6(c) and 6(d)]; PMA was increased or decreased with an increase in t_{MnPd} at lower and higher temperatures, respectively, because the levels of perpendicular crystalline anisotropy of interfacial moments were different. Our results demonstrate how various $Mn_{1-x}Pd_x$ alloy films can trigger PMA in adjacent FM films. We revealed that $Mn_{0.9}Pd_{0.1}$ films, which have both high AFM moments and valence orbitals, can be used to enhance PMA in Co/Ni/Cu films through the dual effects of exchange and spin-orbit coupling. This application may also be extended to thicker $Mn_{1-x}Pd_x$ films with higher Pd concentration or other AFM–noble-metal alloys to offer an additional degree of freedom in controlling the PMA of FM films. The direct applications of the proposed systems in perpendicular magnetic tunnel junctions may be limited by the unsolved problems of structural incompatibility precluding body-centered-cubic (MgO) and fcc-like $Mn_{1-x}Pd_x$ electrodes and diffusion occurring after thermal annealing; nevertheless, our findings indicate the critical conditions and mechanisms of alloying or doping AFM films with a noble metal to induce PMA in FM layers with different levels of in-plane magnetic anisotropy.

V. CONCLUSION

We comprehensively investigated and characterized the ability of a series of AFM $Mn_{1-x}Pd_x$ films to induce PMA in two types of FM films (Co/Ni/Cu and Co/Fe/Cu). $Mn_{1-x}Pd_x$ films can trigger PMA in a Co/Ni/Cu film with weak in-plane magnetic anisotropy at room temperature through $Mn_{1-x}Pd_x$-facilitated interfacial perpendicular crystalline anisotropy (spin-orbit coupling; $x \geqslant 10\%$) or incorporation of them with antiferromagnet-induced exchange coupling ($x \leqslant 10\%$). In a Co/Fe/Cu film with strong in-plane magnetic anisotropy, stable PMA can only be induced by Mn-rich $Mn_{1-x}Pd_x$ films ($x \leqslant 10\%$) at low temperatures through concurrently enhanced perpendicular crystalline anisotropy and antiferromagnet-induced exchange coupling across the AFM–FM interface. Our study demonstrates the dual effects of the spin-orbit and exchange coupling of $Mn_{1-x}Pd_x$ films in triggering PMA in adjacent FM films, indicating that $Mn_{1-x}Pd_x$ films are promising candidates for controllable PMA. These findings are crucial for understanding the critical conditions and mechanisms of noble-metal alloying or doping effects on antiferromagnet-induced PMA, which can inspire the application of PMA in next-generation perpendicular spintronic devices consisting of AFM films with noble-metals elements.

[1] C. Chappert, A. Fert, and F. N. Van Dau, Nat. Mater. **6**, 813 (2007).

[2] S. Ikeda, K. Miura, H. Yamamoto, K. Mizunuma, H. D. Gan, M. Endo, S. Kanai, J. Hayakawa, F. Matsukura, and H. Ohno, Nat. Mater. **9**, 721 (2010).

[3] W.-G. Wang, M. Li, S. Hageman, and C. L. Chien, Nat. Mater. **11**, 64 (2012).

[4] G. Yu, P. Upadhyaya, Y. Fan, J. G. Alzate, W. Jiang, K. L. Wong, S. Takei, S. A. Bender, L. Chang, Y. Jiang, M. Lang, J. Tang, Y. Wang, Y. Tserkovnyak, P. K. Amiri, and K. L. Wang, Nat. Nanotechnol. **9**, 548 (2014).

[5] F. A. Cuellar, Y. H. Liu, J. Salafranca, N. Nemes, E. Iborra, G. Sanchez-Santolino, M. Varela, M. G. Hernandez, J. W. Freeland, M. Zhernenkov, M. R. Fitzsimmons, S. Okamoto, S. J. Pennycook, M. Bibes, A. Barthélémy, S. G. E. Te Velthuis, Z. Sefrioui, C. Leon, and J. Santamaria, Nat. Commun. **5**, 4215 (2014).

[6] D. C. Worledge, G. Hu, D. W. Abraham, J. Z. Sun, P. L. Trouilloud, J. Nowak, S. Brown, M. C. Gaidis, E. J. O'Sullivan, and R. P. Robertazzi, Appl. Phys. Lett. **98**, 022501 (2011).

[7] N. Nakajima, T. Koide, T. Shidara, H. Miyauchi, H. Fukutani, A. Fujimori, K. Iio, T. Katayama, M. Nývlt, and Y. Suzuki, Phys. Rev. Lett. **81**, 5229 (1998).

[8] M. T. Johnsony, P. J. H. Bloemenzx, F. J. A. den Broeder, and J. J. de Vries, Rep. Prog. Phys. **59**, 1409 (1996).

[9] T. Burkert, L. Nordström, O. Eriksson, and O. Heinonen, Phys. Rev. Lett. **93**, 027203 (2004).

[10] A. Winkelmann, M. Przybylski, F. Luo, Y. Shi, and J. Barthel, Phys. Rev. Lett. **96**, 257205 (2006).

[11] B.-Y. Wang, C.-Y. Hsu, B.-X. Liao, Y.-L. Hsu, Y.-M. Lai, M.-S. Tsai, T.-H. Chuang, and D.-H. Wei, Phys. Rev. B **104**, 174407 (2021).

[12] J. Stöhr and H. C. Siegmann, *Magnetism: From Fundamentals to Nanoscale Dynamics* (Springer, New York, 2006).

[13] B. Y. Wang, N. Y. Jih, W. C. Lin, C. H. Chuang, P. J. Hsu, C. W. Peng, Y. C. Yeh, Y. L. Chan, D. H. Wei, W. C. Chiang, and M. T. Lin, Phys. Rev. B **83**, 104417 (2011).

[14] B. Y. Wang, J. Y. Hong, K. H. O. Yang, Y. L. Chan, D. H. Wei, H. J. Lin, and M. T. Lin, Phys. Rev. Lett. **110**, 117203 (2013).

[15] P. Kuświk, P. L. Gastelois, M. M. Soares, H. C. N. Tolentino, M. De Santis, A. Y. Ramos, A. D. Lamirand, M. Przybylski, and J. Kirschner, Phys. Rev. B **91**, 134413 (2015).

[16] P. Kuświk, B. Szymański, B. Anastaziak, M. Matczak, M. Urbaniak, A. Ehresmann, and F. Stobiecki, J. Appl. Phys. **119**, 215307 (2016).

[17] B.-Y. Wang, P.-H. Lin, M.-S. Tsai, C.-W. Shih, M.-J. Lee, C.-W. Huang, N.-Y. Jih, P.-Y. Cheng, and D.-H. Wei, Phys. Rev. B **92**, 214435 (2015).

[18] B.-Y. Wang, M.-S. Tsai, C.-W. Huang, C.-W. Shih, C.-J. Chen, K. Lin, J.-J. Li, N.-Y. Jih, C.-I. Lu, T.-H. Chuang, and D.-H. Wei, Phys. Rev. B **96**, 094416 (2017).

[19] B.-Y. Wang, C.-H. Hsiao, B.-X. Liao, C.-Y. Hsu, T.-H. Li, Y.-L. Hsu, Y.-M. Lai, M.-S. Tsai, T.-H. Chuang, and D.-H. Wei, Phys. Rev. B **104**, 024424 (2021).

[20] B.-Y. Wang, J.-Y. Ning, T.-H. Li, C.-C. Chung, C.-Y. Hsu, M.-S. Tsai, T.-H. Chuang, and D.-H. Wei, Phys. Rev. B **105**, 184415 (2022).

[21] N. Y. Jih, B. Y. Wang, Y. L. Chan, D. H. Wei, and M. T. Lin, Appl. Phys. Express **5**, 063008 (2012).

[22] B. Y. Wang, C. C. Chiu, W. C. Lin, and M. T. Lin, Appl. Phys. Lett. **103**, 042407 (2013).

[23] T. Ambrose and C. L. Chien, Phys. Rev. Lett. **76**, 1743 (1996).

[24] J. S. Kouvel and J. S. Kasper, J. Phys. Chem. Solids **24**, 529 (1963).

[25] H. Umebayashi and Y. Ishikawa, J. Phys. Soc. Jpn. **21**, 1281 (1966).

[26] W. Kuch, L. I. Chelaru, F. Offi, J. Wang, M. Kotsugi, and J. Kirschner, Phys. Rev. Lett. **92**, 017201 (2004).

[27] M. Ekholm and I. A. Abrikosov, Phys. Rev. B **84**, 104423 (2011).

[28] P. J. Hsu, C.-I. Lu, Y. H. Chu, B. Y. Wang, C. B. Wu, L. J. Chen, S. S. Wong, and M. T. Lin, Phys. Rev. B **85**, 174434 (2012).

[29] C. B. Wu, J. Song, and W. Kuch, Appl. Phys. Lett. **101**, 012404 (2012).

[30] H. P. J. Wijn, *Magnetic Properties of Metals* (Springer, New York, 1991), p. 83.

[31] L. Pál, E. Krén, G. Kádár, P. Szabó, and T. Tarnóczi, J. Appl. Phys. **39**, 538 (1968).

[32] E. Krén and J. Solyom, Phys. Lett. **22**, 273 (1966).

[33] J. Okabayashi, Y. Miura, and H. Munekata, Sci. Rep. **8**, 8303 (2018).

[34] N. Cheng, J. Ahn, and K. M. Krishnan, J. Appl. Phys. **89**, 6597 (2001).

[35] P. Blomqvist and K. M. Krishnan, J. Appl. Phys. **95**, 8019 (2004).

[36] S. Brück, G. Schütz, E. Goering, X. Ji, and K. M. Krishnan, Phys. Rev. Lett. **101**, 126402 (2008).

[37] J. S. Jeong, Z. Akase, D. Shindo, Q.-f. Zhan, and K. M. Krishnan, J. Electron Microsc. **60**, 235 (2011).

[38] B. Schulz and K. Baberschke, Phys. Rev. B **50**, 13467 (1994).

[39] R. F. Willis, J. A. C. Bland, and W. Schwarzacher, J. Appl. Phys. **63**, 4051 (1988).

[40] J. Shen, A. K. Swan, and J. F. Wendelken, Appl. Phys. Lett. **75**, 2987 (1999).

[41] See Supplemental Material at http://link.aps.org/supplemental/10.1103/PhysRevB.107.104429 for information on the growth, crystalline structure of the $Mn_{1-x}Pd_x$ films on 2-ML Co/14-ML Ni/Cu(001) and 3-ML Co/3-ML Fe/Cu(001), and magnetic anisotropy energy density of 2-ML Co/14-ML Ni/Cu(001), and 3-ML Co/3-ML Fe/Cu(001).

[42] The lattice mismatch between Cu(001) and bulk MnPd(001) [or Pd(001)] are approximately -12.7% [30] (or -7.7%) (see Refs. [43,44]).

[43] D. P. Woodruff and E. Vlieg, *Surface Alloys and Alloy Surfaces*, edited by D. P. Woodruff (Elsevier, Amsterdam, 2002).

[44] L. Vitos, A. V. Ruban, H. L. Skriver, and J. Kollar, Surf. Sci. **411**, 186 (1998).

[45] C. T. Chen, Y. U. Idzerda, H. J. Lin, N. V. Smith, G. Meigs, E. Chaban, G. H. Ho, E. Pellegrin, and F. Sette, Phys. Rev. Lett. **75**, 152 (1995).

[46] J. Stöhr, Y. Wu, B. D. Hermsmeier, M. G. Samant, G. R. Harp, S. Koranda, D. Dunham, and B. P. Tonner, Science **259**, 658 (1993).

[47] C. M. Schneider and G. Schönhense, Rep. Prog. Phys. **65**, 1785 (2002).

[48] D.-H. Wei, Y.-L. Chan, and Y.-J. Hsu, J. Electron Spectrosc. Relat. Phenom. **185**, 429 (2012).

[49] A. Scholl, J. Stöhr, J. Lüning, J. W. Seo, J. Fompeyrine, H. Siegwart, J. P. Locquet, F. Nolting, S. Anders, E. E. Fullerton, M. R. Scheinfein, and H. A. Padmore, Science **287**, 1014 (2000).

[50] F. Nolting, A. Scholl, J. Stöhr, J. W. Seo, J. Fompeyrine, H. Siegwart, J. P. Locquet, S. Anders, J. Lüning, E. E. Fullerton, M. F. Toney, M. R. Scheinfein, and H. A. Padmore, Nature (London) **405**, 767 (2000).

[51] H. Ohldag, A. Scholl, F. Nolting, S. Anders, F. U. Hillebrecht, and J. Stöhr, Phys. Rev. Lett. **86**, 2878 (2001).

[52] W. Kim, E. Jin, J. Wu, J. Park, E. Arenholz, A. Scholl, C. Hwang, and Z. Q. Qiu, Phys. Rev. B **81**, 174416 (2010).

[53] W. J. Antel, Jr., F. Perjeru, and G. R. Harp, Phys. Rev. Lett. **83**, 1439 (1999).

[54] J. Nogués and I. K. Schuller, J. Magn. Magn. Mater. **192**, 203 (1999).

[55] F. Offi, W. Kuch, and J. Kirschner, Phys. Rev. B **66**, 064419 (2002).

[56] C. Won, Y. Z. Wu, H. W. Zhao, A. Scholl, A. Doran, W. Kim, T. L. Owens, X. F. Jin, and Z. Q. Qiu, Phys. Rev. B **71**, 024406 (2005).

[57] K. Lenz, S. Zander, and W. Kuch, Phys. Rev. Lett. **98**, 237201 (2007).

[58] P. Bruno, Phys. Rev. B **39**, 865 (1989).

[59] J. Stöhr and H. König, Phys. Rev. Lett. **75**, 3748 (1995).

[60] B. T. Thole, P. Carra, F. Sette, and G. van der Laan, Phys. Rev. Lett. **68**, 1943 (1992).

[61] P. Carra, B. T. Thole, M. Altarelli, and X. Wang, Phys. Rev. Lett. **70**, 694 (1993).

[62] R. Wu, D. Wang, and A. J. Freeman, Phys. Rev. Lett. **71**, 3581 (1993).

[63] E. C. Stoner and E. P. Wohlfarth, Philos. Trans. R. Soc. London A **240**, 599 (1948).

[64] S. Peng, W. Zhao, J. Qiao, L. Su, J. Zhou, H. Yang, Q. Zhang, Y. Zhang, C. Grezes, P. K. Amiri, and K. L. Wang, Appl. Phys. Lett. **110**, 072403 (2017).

[65] According to Néel type phenomenological magnetic anisotropy model [75], the surface magnetic anisotropy energy contributed by 1 ML Mn was estimated roughly to be approximately 0.64 mJ/m^2 [41].

[66] F. Offi, W. Kuch, L. I. Chelaru, K. Fukumoto, M. Kotsugi, and J. Kirschner, Phys. Rev. B **67**, 094419 (2003).

[67] M. Kowalewski, C. M. Schneider, and B. Heinrich, Phys. Rev. B **47**, 8748 (1993).

[68] W. C. Lin, C. C. Kuo, C. L. Chiu, and M.-T. Lin, J. Appl. Phys. **89**, 7139 (2001).

[69] F. E. Gabaly, K. F. McCarty, A. K. Schmid, J. de la Figuera, M. C. Muñoz, L. Szunyogh, P. Weinberger, and S. Gallego, New J. Phys. **10**, 073024 (2008).

[70] A slight reduction of the critical temperature of 175 K in $Mn_{0.9}Pd_{0.1}$/Co/Fe/Cu [Fig. 6(d)], compared to 185 K in Mn/Co/Fe/Cu [Fig. 6(c)], may be attributed to the lower thermal stability of the established noncollinear exchange coupling.

[71] C. L. Gao, A. Ernst, A. Winkelmann, J. Henk, W. Wulfhekel, P. Bruno, and J. Kirschner, Phys. Rev. Lett. **100**, 237203 (2008).

[72] J. Dresselhaus, D. Spanke, F. U. Hillebrecht, E. Kisker, G. van der Laan, J. B. Goedkoop, and N. B. Brookes, Phys. Rev. B **56**, 5461 (1997).

[73] T. J. Jicks, A. R. Pepper, and J. H. Smith, J. Phys. C **1**, 1683 (1968).

[74] T. Hori, Y. Tsuchiya, Y. Ishii, and K. Hojou, Mater. Trans. **43**, 436 (2002).

[75] L. Néel, C. R. Acad. Sci. **237**, 1468 (1953); J. Phys. Radium **15**, 225 (1954).